International Journal of GEOMATE, Sep., 2024 Vol.27, Issue 121, pp.69-76
ISSN: 2186-2982 (P), 2186-2990 (O), Japan, DOI: https://doi.org/10.21660/2024.121.4517
Geotechnique, Construction Materials and Environment

NOVEL APPLICATION OF MODEL UPDATING FOR DAMAGE DETECTION OF UHPC XUAN DUC BRIDGE

Quoc-Bao Nguyen[1] and *Thi-Nguyet-Hang Nguyen[1]

[1]Department of Bridge and Road Engineering, Hanoi University of Civil Engineering, Vietnam

*Corresponding Author, Received: 02 April 2024, Revised: 24 June 2024, Accepted: 29 June 2024

ABSTRACT: This article introduces an innovative approach to assess the structural health of bridges based on dynamic and static load test data from the Xuan Duc bridge, a bridge constructed using Ultra-High-Performance Concrete (UHPC) in Tuyen Quang Province, Vietnam. The measured deflection values of all girders and the natural frequency of the superstructure, along with the PSO (Particle Swarm Optimization) algorithm, were employed to update a finite element model developed in SAP2000 (a commercial structural analysis and design software). This updating process resulted in a significant reduction in error from 5.81% to 0.22% for deflection values and from 2.48% to 0.02% for natural frequencies when compared with the measured data. It is shown that the updated numerical model accurately reflects the operational condition of the bridge during load testing, facilitating the determination of the elastic modulus values of UHPC material. Additionally, this paper explores the feasibility of the approach in identifying the location and degree of damage in superstructures by conducting two numerical case studies with high accuracy. Furthermore, the effect of noise in load testing on the updating process was also considered. With a maximum noise level of 3%, the method maintains accuracy in locating damaged zones, yielding damage level values of 24.70% and 36.47% compared to respective 20% and 30% without noise. Results from this paper confirm the effectiveness of applying machine learning in advanced structural health monitoring.

Keywords: UHPC, Damage Detection, Bridge Load Test, Optimization Algorithm

1. INTRODUCTION

In contemporary society, the expansion of both industrial and service sectors necessitates the rapid advancement of road transport networks. Within this intricate system, bridges used to overcome obstacles are typically constructed from reinforced concrete, steel, and, more recently, Ultra-High Performance Concrete (UHPC) materials. Design standards such as the American Association of State Highway and Transportation Officials (AASHTO) and European standards (EUROCODE) [1, 2], etc., are adhered to meticulously to ensure the structural integrity and safety of these vital components throughout their projected lifespan. However, various factors, including overloaded exploitation and collisions with ships, barges, trucks, etc., pose significant risks to the durability, longevity, and overall safety of bridges. Incidents resulting from such risks can lead to substantial financial losses and, more importantly, human casualties [3]. To mitigate these risks effectively, it is imperative to conduct regular monitoring and evaluation of bridge structures. By promptly detecting any signs of damage, necessary repairs can be undertaken to minimize the likelihood of major structural issues and consequent repair costs [4]. Such proactive measures not only enhance safety but also optimize the construction and exploitation of bridge infrastructure, ensuring its continued functionality and resilience.

Several methods are employed for this purpose, ranging from visual inspections to advanced structural health monitoring techniques. Visual inspections involve a physical examination of bridge components, looking for signs of distress such as cracks, spalling, or corrosion [5-8]. While effective for identifying surface-level damage, visual inspections may not uncover internal or hidden defects. Non-destructive testing (NDT) methods offer a more comprehensive approach to bridge assessment. Techniques such as ultrasonic testing, ground-penetrating radar, and magnetic flux leakage can detect internal defects and assess the condition of bridge elements without causing harm to the structure. These methods provide valuable insights into the integrity of the bridge, enabling engineers to identify potential issues early on [9-12]. Structural health monitoring (SHM) systems represent the cutting edge of bridge damage detection. These systems utilize sensors embedded within the structure to continuously monitor its behavior and performance. By collecting data on factors such as strain, vibration, and temperature, SHM systems can detect anomalies indicative of damage or deterioration. Advanced analytics and machine learning algorithms further enhance the capabilities of SHM, allowing for predictive maintenance and real-time assessment of bridge conditions [13-18].

Nguyen and Do [19] utilized load test data and an optimization algorithm to successfully update the elastic modulus of a simple supported span bridge featuring a cross-section comprising six I-shaped

main beams. This study also evaluated and compared the bridge construction conditions before and after retrofitting. Saleh et al. [14] used a numerical algorithm using Frequency Response Functions (FRFs) data to calculate the different FRFs for undamaged and damaged beam conditions to determine damage index and crack damage in reinforced concrete beams. Doubling et al. [17] showed an overview of methods to identify the location and characteristics of damages in structures by investigating changes in measured vibration responses. Hassani and Dackermann [20] conducted a systematic review of optimization algorithms for SHM and optimal sensor placement and showed that using optimization algorithms in machine learning allows users to find the best available values of an objective function given a specific domain. The research demonstrates that artificial intelligence (AI) holds the potential to deliver both high accuracy and swift results in tackling intricate engineering structural issues. Prior investigations have indicated a variety of research endeavors utilizing data from SHM and optimization algorithms to forecast on-site conditions for various bridge types, including reinforced concrete, prestressed reinforced concrete, and steel bridges. Nevertheless, it is essential to acknowledge a recent surge in the utilization of Ultra-High Performance Concrete (UHPC) materials. UHPC stands out due to its remarkable compressive strength, heightened ductility, and exceptional resistance to corrosion and abrasion. Employing UHPC not only fosters sustainability by curbing material consumption but also minimizes the necessity for future repairs and maintenance [21]. Consequently, an increasing number of UHPC bridges are being erected worldwide. However, owing to the novelty of these UHPC bridges in comparison to other bridge types, further research and experimental data are imperative to enhance our understanding of this type of bridge.

This article presents static load test data (beam deflection) and dynamic load test data (natural frequency) measured from SHM for UHPC Xuan Duc Bridge. In addition, a finite element (FE) model established in SAP2000 to trace the on-site behavior of the bridge's superstructure is developed. Based on the load test results (beam deflection and natural frequency), the numerical model was then updated using the Particle Swarm Optimization (PSO) algorithm. The updated model's values for beam deflections and natural frequencies closely matched those obtained from the load test. Thus, the updated numerical model accurately reflects the state of the bridge structure at the time of the load test, ensuring that the elastic modulus used in the FE model is consistent with that of the bridge structure during the load testing phase. Furthermore, updating the numerical model facilitates the identification of the location and the degree of damage within a damaged zone of the beam. Several case studies employing numerical methods were conducted, demonstrating the potential to detect damage based on bridge load test data. Additionally, the article delves into the analysis of how measurement noise impacts the damage determination process.

2. RESEARCH SIGNIFICANCE

In this study, the PSO optimization algorithm is employed to update the numerical model using the findings from static load and dynamic load tests. The updated numerical model accurately represents the current operational condition of the bridge structure, facilitating the determination of the elastic modulus of the UHPC beam. Additionally, updating the model enables the identification of the location and degree of damage within a beam segment under the assumption that all other zones remain undamaged. Furthermore, an analysis of measurement noise was conducted to showcase the practical viability of this approach.

3. DESCRIPTION OF XUAN DUC BRIDGE

The Xuan Duc Bridge is situated in Xuan Duc village, Hung Duc commune, Ham Yen district, Tuyen Quang province, Vietnam. The total length of this bridge is 21.04 m, comprising a single simply supported span. The lengths of the two abutments are 4 m and 5 m, respectively. The total width of the two expansion joints is 40 mm (20 mm × 2), and the beam length is 12 m (refer to Fig.1a). The overall width of this bridge is 4 m, with the vehicle lane measuring 3.5 m in width and each railing measuring 0.25 m in width. The superstructure's cross-section consists of two prefabricated beams in a Π shape constructed from prestressed UHPC. Each beam has a height of 0.4 m, a width of 1.95 m, and a rib spacing of 1 m. The slab thickness is 65 mm, with the main beam rib varying in width from 140 mm to 190 mm (refer to Fig.1b and c). Each Π beam is equipped with 18 pre-tensioned strands of 12.7 mm type, with 9 strands in each rib (1 above and 8 below). The bridge also features four 185 mm high and 150 mm wide cross-beams situated at the ends, 1/3, and 2/3 of the span. The prefabricated Π beams are joined together at the construction site along the length of the beam. All Π beams, cross-beams, and joints are composed of UHPC material, boasting a specified compressive strength of 130 MPa. The railings, measuring 250×200 mm, are precast in the factory and made from reinforced concrete with a compressive strength of 30 MPa. Epoxy is applied as a surface coating to enhance roughness. The U-shaped bridge abutment is constructed from reinforced concrete with a compressive strength of 30 MPa, with the abutment foundation placed on the natural substrate.

(a) General layout

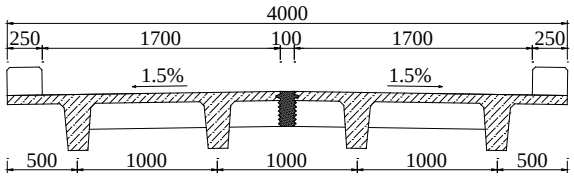

(b) Bridge cross section

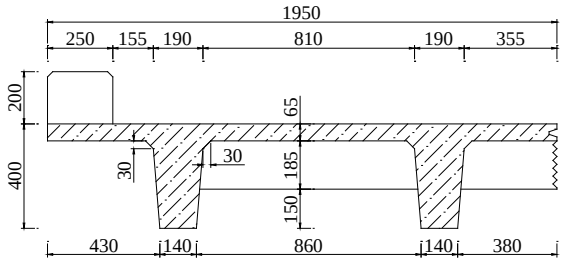

(c) Π beam cross section

Fig.1 Xuan Duc bridge

4. BRIDGE LOAD TESTING AND FE MODEL

4.1 Bridge Load Testing

Xuan Duc Bridge underwent load testing comprising two main components: static load testing and dynamic load testing. The test load consisted of a truck with two axles, positioned with a distance of 3.65 m along the bridge and a transversal distance of 1.85 m between the two wheels (Fig.2a). The total load of this truck, including sand, amounted to 23.25 tons.

Static load test: Four indicators with measurements ranging from 0 to 50 mm were affixed to the bottom of the four beam ribs at the mid-span position (Fig.2b). The difference in indicator readings between when the truck was present on the bridge and when it was absent provided the deflection value caused by the truck. The experimental results are summarized in Table 2.

Dynamic load test: To measure the vibrations of the superstructure, the test truck was driven across the bridge at a velocity of approximately 30 km/h. Vibration data of the superstructure were collected using a digital oscilloscope SDA-830C and a 3-axis accelerometer sensor. Analysis of the vibration measurement results facilitated the determination of the natural frequencies of the superstructure, as depicted in Table 3.

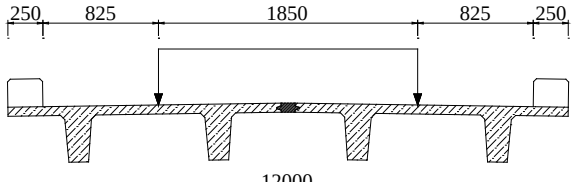

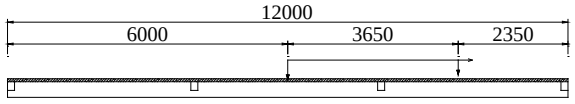

(a) Test truck

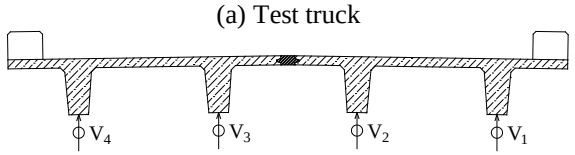

(b) Indicators

Fig.2 Equipment arrangement

4.2 Finite Element Model

The Xuan Duc bridge has been modeled using the finite element method in Sap2000 software [22]. Elastic modulus of the Π beams, cross-beams, and railings are outlined in Table 1, corresponding to the case before updating the numerical model. These values are referenced in the Xuan Duc bridge design documents provided by the Department of Transport of Tuyen Quang. Each Π beam rib and slab within 1 m is represented by a beam element. Beam elements are also utilized to model cross-beams and railings. The boundary condition of the Π beams was set as simply supported. The test truck was simulated as static concentrated loads acting on the superstructure, enabling the determination of the deflection of each Π beam rib. The numerical model of the Xuan Duc bridge is illustrated in Fig.3.

Table 2 presents the deflection values of the superstructure (y_1, y_2, y_3, and y_4 are deflections of four beam ribs) under the impact of the truck. The deflections of the two outer beam ribs obtained from the FE model before updating exhibit errors compared to the load test results of 5.14% and 5.17%, respectively. Meanwhile, these error values increase for the two inner beam ribs, amounting to 5.81% and 5.75%. This discrepancy can arise when the ratios of the elastic modulus of the railing are divided by the elastic modulus of the beam in the numerical model before updating and the experimental model differs.

Fig.4 and Table 3 illustrate the vibration modes of the first two bending vibration modes and their corresponding natural frequencies. The results of the

load test model and the numerical model before updating reveal that the values of natural frequencies of these two models are significant, with errors of 2.48% and 1.80% for the 1st vertical bending mode and the 2nd vertical bending mode. Therefore, the material characteristics of the left railing, right railing, left Π beam, and right Π beam need to be accurately updated. Once updated, the numerical model can accurately represent the bridge condition at the time of the load test survey.

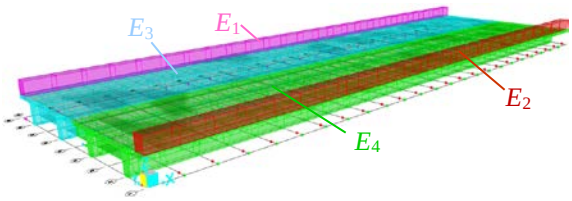

Fig.3 FE model and updated parameters

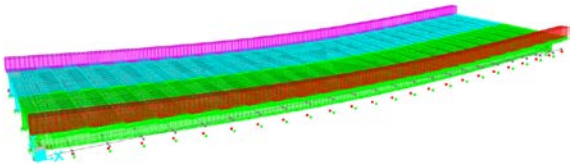

(a) Mode 1: f_1 = 5.423 Hz

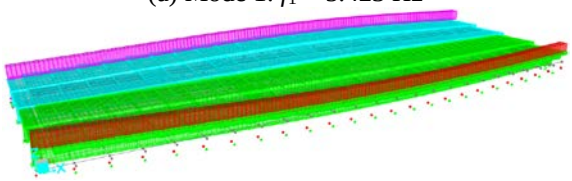

(b) Mode 2: f_2 = 7.121 Hz

Fig.4 First two modes of the FE model of the Xuan Duc bridge before updating

Table 1. Elastic modulus based on numerical and experimental models

	Elastic modulus (MPa)			
	E_1	E_2	E_3	E_4
Before updating	28111	28111	45000	45000
After updating	27956 (0.55%)	27937 (0.62%)	49023 (8.94%)	49017 (8.93%)

Note: E_1, E_2 represent the elastic modulus of the railings on the left and right side; E_3, E_4 represent the elastic modulus of the beam on the left and right side; Values in the parentheses indicate errors compared to data before updating.

Table 2. Beam rib deflection based on numerical and experimental models

	Deflection (mm)			
	y_1	y_2	y_3	y_4
Experimental data	-13.782	-14.611	-14.619	-13.778
Before updating	-14.490 (5.14%)	-15.459 (5.81%)	-15.459 (5.75%)	-14.490 (5.17%)
After updating	-13.751 (0.22%)	-14.626 (0.11%)	-14.627 (0.05%)	-13.752 (0.19%)

Note: Values in the parentheses indicate errors compared to experimental data.

Table 3. Natural frequencies based on numerical and experimental models

	Natural frequencies (Hz)	
	1st vertical bending	2nd vertical bending
Experimental data	5.561	7.251
Before updating	5.423 (2.48%)	7.121 (1.80%)
After updating	5.557 (0.07%)	7.253 (0.02%)

Note: Values in the parentheses indicate errors compared to experimental data.

5. MODEL UPDATING OF XUAN DUC BRIDGE PARAMETERS

The results of natural frequencies and deflection of beam ribs in Table 2 and Table 3 reveal a significant difference between the experimental model and the numerical model. Thus, the numerical model needs updating to accurately reflect the experimental model. Because the two Π beams were poured separately, there may be differences in material properties, similarly for the concrete railings. Therefore, this article proposes updating the following four characteristics, as shown in Fig.3:

- E_1, E_2 represent the elastic modulus of the railings on the left and right sides, respectively;
- E_3, E_4 represent the elastic modulus of the beams on the left and right sides.

The four elastic moduli mentioned above can be accurately determined (updated) through optimization algorithms based on experimental data (the first two natural frequencies and the deflection at the mid-span position of four beam ribs) as described above. Various optimization algorithms have been proposed and applied in different fields, such as the Particle Swarm Optimization (PSO), Genetic Algorithm (GA), and Cuckoo Algorithm [23-26]. In this article, the PSO algorithm was employed to solve the problem. The PSO algorithm (Particle Swarm Optimization) was introduced by Kennedy, J. and R. Eberhart in 1985 [24, 26]. This algorithm was developed based on the following assertion: during the random search for food, some birds may share what they find with the entire flock so that the entire flock can benefit, leading to better hunting results. The PSO algorithm can be described as follows:

- The initial position of the birds is randomly initialized within a predetermined constraint range, and from there, the value of the objective function can be calculated.

- The best location for each bird and for the entire flock at this time is determined.
- The position of each bird is updated depending on the two best positions mentioned above.
- This process repeats until a certain objective function value is reached or after a certain number of iterations.

The objective function utilized in this study follows the formulation proposed by Nguyen and Do [19]. It includes the values of the first two natural frequencies and the deflection of the four beam ribs, as represented by Eq. (1) below:

$$\text{Objective function} = \sum_{i=1}^{2}\left[\frac{f_{Exp}^{i}-f_{FE}^{i}}{f_{Exp}^{i}}\right]^{2}\times\omega_{dyn}+\sum_{j=1}^{4}\left[\frac{y_{Exp}^{j}-y_{FE}^{j}}{y_{Exp}^{j}}\right]^{2}\times\omega_{sta} \quad (1)$$

where:

- f_{Exp}^{i}, f_{FE}^{i}: the first two natural frequencies of the experimental model and numerical model, respectively;
- y_{Exp}^{j}, y_{FE}^{j}: the deflection at the mid-span position of four beam ribs of the experimental model and numerical model, respectively;
- $\omega_{dyn}, \omega_{sta}$: the weight parameters assigned to the dynamic results and static results, respectively, depending on the level of accuracy between them. In this study, $\omega_{dyn}=1$ and $\omega_{sta}=0.1$ as used in Nguyen and Do [19] are adopted.

The lower and upper bound values of the elastic modulus are shown in Table 4. Based on the experimental data of the first two natural frequencies and the deflections at the mid-span position of the four beam ribs, summarized in Table 3 and Table 2, the elastic modulus values in the numerical model are updated, as shown in Table 1, corresponding to the case after updating the numerical model. The values of deflections after model updating are also summarized in Table 2, while the values of natural frequencies after model updating are shown in Table 3.

Consequently, the errors of the first two bending natural frequencies obtained from the numerical model compared to the experiment before updating are 2.48% and 1.80%, respectively. These values decrease significantly after updating, to 0.07% and 0.02%, respectively, showing a considerable improvement from before updating. Similarly, the error values of the deflections of the four beam ribs before updating are 5.14%, 5.81%, 5.75%, and 5.17%. These values also decrease substantially after updating, by 0.22%, 0.11%, 0.05%, and 0.19%, respectively. Additionally, the objective function value decreases from 2.14×10^{-3} to 1.61×10^{-6}, corresponding to a reduction of more than 1300 times (this value decreases rapidly in about the first 10 iterations). The objective function value for the first 1000 iterations is illustrated in Fig.5 (the inset shows the value for the last 200 iterations).

Table 4. Variation range of elastic modulus in the FE model

Range	Elastic modulus (MPa)			
	E_1	E_2	E_3	E_4
Lower	0	0	0	0
Upper	60000	60000	60000	60000

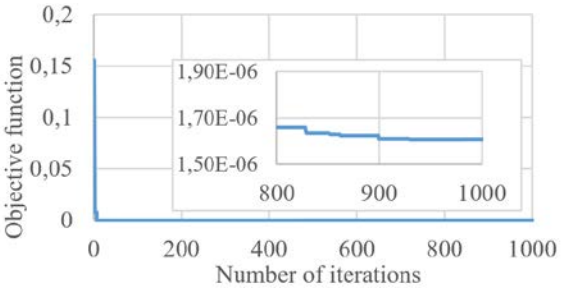

Fig.5 Objective function vs. number of iterations

6. DETECT DAMAGES ON THE UHPC PI BEAM

6.1 Case Studies: Reference Cases

The process of updating the numerical model in Section 5 allows for the determination of the elastic modulus values of the beams and railings. Additionally, the change in the elastic modulus value reflects the alteration in the beam stiffness value, which is equivalent to the product of the elastic modulus and moment of inertia. This prompts consideration of the possibility of identifying damaged zones in bridge structures after updating the elastic modulus based on dynamic and static measurement data. This section investigates the feasibility of this method through numerical modeling analyses. Two case studies are provided in Table 5 and described as follows:

- Case study 1 (CS1): One instance of damage occurred between 1/4 and 1/2 of the 3rd beam from the left side (inner rib). The deterioration condition is depicted by the reduction in elastic modulus. In this scenario, the stiffness of the damaged beam segment decreases by 20% compared to the remaining beam segments.
- Case study 2 (CS2): One damage occurred between 1/2 and 3/4 of the 1st beam from the left side (outer rib). The stiffness of the damaged beam segment is 70% of that of the remaining beam segments (corresponding to a 30% decrease in stiffness).

The degree of damage is expressed by the decrease in the elastic modulus value at these beam

segments. The values of natural frequencies and deflection of beam ribs from the numerical model are summarized in Table 5, serving as reference values for determining damage in the subsequent section.

Table 5. Reference data vs data after updating for CS1 and CS2 – Elastic modulus

Case study	Elastic modulus (MPa)		Position of the damage beam segment
	Intact beam segment	Damage beam segment	
Reference data / Assumed data			
CS1	49023.00	39218.40	1/4-1/2 of 3rd beam rib
CS2	49023.00	34311.90	1/2-3/4 of 1st beam rib
After updating			
CS1	49017.16 (0.012%)	39233.84 (0.039%)	1/4-1/2 of 3rd beam rib
CS2	49019.46 (0.007%)	34315.03 (0.009%)	1/2-3/4 of 1st beam rib

Note: Values in the parentheses indicate errors compared to reference data.

Table 6. Reference data vs data after updating for CS1 and CS2 – deflection and natural frequencies

Case study	Deflection (mm)			
	y_1	y_2	y_3	y_4
Reference data / Assumed data				
CS1	-13.8973	-14.8477	-14.9268	-13.9931
CS2	-14.3258	-15.0224	-14.8618	-13.8665
After updating				
CS1	-13.8973 (0.000%)	-14.8476 (0.000%)	-14.9268 (0.000%)	-13.9932 (0.001%)
CS2	-14.3229 (0.020%)	-15.0202 (0.014%)	-14.8605 (0.009%)	-13.8658 (0.005%)
Case study	Natural frequencies (Hz)			
	1st vertical bending		2nd vertical bending	
Reference data				
CS1	5.5237		7.2365	
CS2	5.4972		7.2088	
After updating				
CS1	5.5237 (0.000%)		7.2365 (0.001%)	
CS2	5.4975 (0.006%)		7.209 (0.003%)	

Note: Values in the parentheses indicate errors compared to reference data.

6.2 Damage Identification

To determine the location and degree of damage for Case studies CS1 and CS2, each beam rib (including the beam rib and bridge deck) among the four beam ribs of the two Π beams is divided into four equal segments. Consequently, there are 16 distinct beam segments with 16 elastic modulus values considered as uncertain parameters. However, with only four rib beam deflection measurements and the first two natural frequencies available, updating all 16 elastic modulus values proves to be exceedingly challenging. Therefore, given the limited experimental data, this present article considers that among the 16 beam segments mentioned above, only one beam segment has reduced stiffness, while the remaining 15 beam segments maintain equal stiffness. Thus, the number of uncertain parameters that need updating in the numerical model will be reduced to three, including the elastic modulus of 15 intact beam segments, the elastic modulus of a beam segment with reduced stiffness, and the location of damage.

After updating the numerical model, the deflection values of the four beam ribs, the first two natural frequencies, the elastic modulus of the intact beam rib, the elastic modulus of the beam segment with reduced stiffness, and the location of this beam segment are summarized in Table 5 and Table 6. For both case studies CS1 and CS2, the results after updating enable accurate determination of the location of damage (stiffness weakness): at the beam segment from 1/4 to 1/2 of 3rd beam rib for CS1, and at the beam segment from 1/2 to 3/4 of 1st beam rib for CS2. The error of the elastic modulus of the intact beam and the damaged beam segment between the two cases after updating and the reference case is very small, less than 0.04%. Additionally, the results of deflections and natural frequencies of the updated model closely align with those of the reference case, with the largest error being 0.02%. Finally, the degrees of damage (defined as the difference of one with the ratio of the elastic modulus of the damaged beam divided by the one of the intact beam) after updating are equal to 19.96% and 29.99% for cases CS1 and CS2, respectively, almost identical to the assumed data.

6.3 Noise Analysis

Model updating for the two cases CS1 and CS2 yields nearly accurate results for determining the location and degree of damage. However, in reality, measurements of deflection and natural frequency contain noise (errors). To assess the influence of noise on the results, the steps outlined in Section 6.2 will be repeated with case studies CS3 and CS4 (which correspond to respective cases CS1 and CS2 with a maximum measurement error of 3%). Updating the numerical model with data on deflection and natural frequency from the reference case is conducted, and the results of this process are summarized in Table 7 and Table 8. With a maximum noise level of 3%, the updated numerical model exhibits a maximum

deflection error of less than 2% for case CS3 and less than 1.8% for case CS4. The error in the natural frequency for both cases CS3 and CS4 is less than 0.5%. The results indicate accurate damage localization for both cases. However, when considering the degree of damage, case CS3 yields a result of 24.70% (compared to the reference case CS1's 20%), and case CS4 yields a result of 36.47% (compared to the reference case CS2's 30%). These findings are deemed acceptable under conditions of 3% noise.

Table 7. Reference data vs data after updating for CS3 and CS4 – deflections and natural frequencies

Case study	Deflection (mm)			
	y_1	y_2	y_3	y_4
Reference data / Assumed data				
CS3	-14.0935	-14.7769	-14.9783	-14.2123
CS4	-14.2770	-15.3028	-14.8922	-14.1910
After updating				
CS3	-13.8199 (1.941%)	-14.777 (0.001%)	-14.8784 (0.667%)	-13.9411 (1.908%)
CS4	-14.5294 (1.768%)	-15.1793 (0.807%)	-14.9736 (0.546%)	-13.9398 (1.770%)
Case study	Natural frequencies (Hz)			
	1st vertical bending		2nd vertical bending	
Reference data				
CS3	5.5312		7.2279	
CS4	5.4958		7.1779	
After updating				
CS3	5.5363 (0.092%)		7.2528 (0.345%)	
CS4	5.4732 (0.412%)		7.1898 (0.166%)	

Note: Values in the parentheses indicate errors compared to reference data.

Table 8. Reference data vs data after updating for CS3 and CS4 – Elastic modulus

Case study	Elastic modulus (MPa)		Position of the damage beam segment
	Intact beam segment	Damage beam segment	
Reference data / Assumed data			
CS3	49023.00	39218.40	1/4-1/2 of 3rd beam rib
CS4	49023.00	34311.90	1/2-3/4 of 1st beam rib
After updating			
CS3	49669.97 (1.320%)	37401.22 (4.633%)	1/4-1/2 of 3rd beam rib
CS4	48784.41 (0.487%)	30990.32 (9.681%)	1/2-3/4 of 1st beam rib

Note: Values in the parentheses indicate errors compared to reference data.

7. CONCLUSIONS

This article presents a novel approach for determining the elastic modulus of bridge beams and assessing damage in bridge structures using load test data. By utilizing data from both static and dynamic load tests, the finite element model of a UHPC bridge was refined through the PSO optimization algorithm. Following the update, this numerical model accurately reflects the bridge's condition during load testing. The updated model yielded deflection values for the four beam ribs with errors not exceeding 0.22% and the first two natural frequencies with the largest error of 0.07% compared to the load test results. Elastic modulus data for UHPC beams were derived from the updated numerical model. Moreover, by updating the numerical model, the article introduces the potential to determine the location and degree of damage in bridge structures based on load test data with relatively high accuracy. Recognizing the presence of noise during load testing, a noise analysis was conducted with a magnitude of 3%. The results obtained were deemed acceptable for accurately determining the location of damage, with damage levels of 24.70% compared to 20% and 36.47% compared to 30%, respectively. Thus, by using load test data (both static and dynamic), updating the numerical model allows for determining the structural condition at the time of the load test, ensuring effective structural health monitoring of bridges.

8. REFERENCES

[1] AASHTO, AASHTO LRFD bridge design specifications. American Association of State Highway and Transportation Officials, Washington DC, 2017, pp: 1.1-15.11.

[2] EN-1992, Eurocode 2: Design of concrete structures, in European Committee for Standardization. Brussels, 2004, pp. 1-87.

[3] Bhattacharya B., 7 - Risk and reliability in bridges, in Innovative Bridge Design Handbook (Second Edition). A. Pipinato, Editor. 2022, Butterworth-Heinemann. pp. 169-213.

[4] Cutrone B., Salvatore W., Renzi E., and Tamasi G., "Guidelines for the classification and management of risk, for the evaluation of safety and for the monitoring of existing bridges". Critical analysis and identification of innovative methods to improve the classification of landslide risk. Procedia Structural Integrity, 2023. 44: pp. 713-720.

[5] Fotouhi S., Pashmforoush F., Bodaghi M., and Fotouhi M., Autonomous damage recognition in visual inspection of laminated composite structures using deep learning. Composite Structures, Vol. 268, 2021, pp. 113960.

[6] Estes A.C., Frangopol D.M., and Foltz S.D.,

Updating reliability of steel miter gates on locks and dams using visual inspection results. Engineering Structures, Vol. 26, Issue 3, 2004, pp. 319-333.
[7] Schoonahd J., Gould J.D., and Miller L.J.E., Studies of visual inspection. Ergonomics, Vol. 16(4), 1973, pp. 365-379.
[8] Jiang X., Gramopadhye A.K., and Melloy B.J., Theoretical issues in the design of visual inspection systems. Theoretical Issues in Ergonomics Science, Vol. 5, Issue 3, 2004, pp. 232-247.
[9] Cheng X., Ma G., Wu Z., Zu H., and Hu X., Automatic defect depth estimation for ultrasonic testing in carbon fiber reinforced composites using deep learning. NDT & E International, Vol. 135, 2023, pp. 102804.
[10] Chen X., Ye Z., Xia J.Y., Wang J.X., and Ji B.H., Double-probe ultrasonic detection method for cracks in steel structure. Applied Sciences, Vol. 10, Issue 23, 2020, pp. 8436.
[11] Yang Y-X., Chai W-H., Liu D-C., Zhang W-D., Lu J-C., and Yang Z-K., An impact-echo experimental approach for detecting concrete structural faults. Advances in Civil Engineering, Vol. 2021, 2021, pp. 1-8.
[12] Dorafshan S. and Azari H., Evaluation of bridge decks with overlays using impact echo, a deep learning approach. Automation in Construction, Vol. 113, 2020, pp. 103133.
[13] Nguyen B.Q., Using optimization algorithms to detect damages on free-free beam based on dynamic results. Journal of Materials Engineering Structures, Vol. 10(3), 2023, pp. 397-414.
[14] Saleh F., Fragomeni S., Tran D., and Prayuda H., Crack detection in reinforced concrete beam structures based on the highest mode shapes subjected to incremental loads. GEOMATE Journal, Vol. 17, Issue 64, 2019, pp. 85-92.
[15] Unno K., Mikami A., and Shimizu M., Damage detection of truss structures by applying machine learning algorithms. GEOMATE Journal, Vol. 16, Issue 54, 2019, pp. 62-67.
[16] Farrar C.R. and Worden K., Structural health monitoring: a machine learning perspective. 2012. John Wiley & Sons, pp.1-631
[17] Doebling S.W., Farrar C., and Prime M.B, A summary review of vibration-based damage identification methods. Engineering, Materials Science, Vol. 30, Issue 2,1998, pp. 91-105.
[18] Koji U., Atsushi M., and Masaki S., Damage detection of truss structures by applying machine learning algorithms. GEOMATE Journal, Vol. 16, Issue 54, 2021, pp. 62-67.
[19] Nguyen D.H. and Do D.V., A novel application to evaluate the bridge health after retrofitting using vibration and static measurements. Journal of Materials Engineering Structures, Vol. 10, Issue 4, 2023, pp. 541-550.
[20] Hassani S. and Dackermann U.J.S., A systematic review of optimization algorithms for structural health monitoring and optimal sensor placement. Sensors (Basel), Vol 23, Issue 6, 2023, pp. 3293.
[21] Abellán-García J., Carvajal-Muñoz J.S., and Ramírez-Munévar C., Application of ultra-high-performance concrete as bridge pavement overlays: Literature review and case studies. Construction and Building Materials, Vol. 410, 2024, pp. 134221.
[22] CSI, SAP 2000 Analysis Reference Manual, in Computers and Structures Inc. 2002: Berkeley, USA.
[23] Mitchell M., An introduction to genetic algorithms. 1998: MIT press, pp. 1-221.
[24] Kennedy J. and Eberhart R., Particle swarm optimization in Proceedings of ICNN'95. International conference on neural networks, Vol. 4, 1995, IEEE, Perth, WA, Australia, pp. 1942-1948.
[25] Yang X-S. and Deb S., Cuckoo search via Lévy flights, World congress on nature & biologically inspired computing (NaBIC), Coimbatore, India, 2009, IEEE, pp. 210-214.
[26] Eberhart R. and Kennedy J., A new optimizer using particle swarm theory. Proceedings of the sixth international symposium on micro machine and human science, Nagoya, 1995, IEEE, pp. 39-43.